PHYSICAL REVIEW A **81**, 022502 (2010)

Effects of valence-valence, core-valence, and core-core correlations on the fine-structure energy levels in Al-like ions

Liang-huan Hao, Gang Jiang,[*] and Hai-jun Hou
Institute of Atomic and Molecular Physics, Sichuan University, 610065, Chengdu, Sichuan, People's Republic of China

(Received 16 July 2009; published 4 February 2010)

This paper reports on multiconfiguration Dirac-Hartree-Fock calculations for both allowed and intercombination transitions and fine structure referring to the levels of a term in highly charged aluminum like ions. Results for fine-structure energy levels, the term splitting, the wavelengths, transition rates, and thereby the branching ratios and lifetimes for the Al-like $3s^2 3p$-$3s3p^2$ transitions in the ions Fe XIV–Au LXVII are reported and compared with other theories and experiments, using the codes GRASP2K. Our calculated fine-structure energy levels are in excellent agreement with the experimental results and the experimentally compiled energy values of the National Institute for Standards and Technology wherever available. The calculated values including core–valence correlation are found to be similar and to compare very well with other theoretical and experimental values for medium-Z ions. For higher Z the inclusion of the valence correlation gives results in excellent agreement with those from many-body perturbation theory. We believe that our extensive calculated values can guide experimentalists in identifying the fine-structure levels in their future work. From our radiative decay rates we have also calculated radiative lifetimes of some fine-structure levels. In this calculation we also predict new data for several fine-structure levels where no other theoretical and/or experimental results are available.

DOI: 10.1103/PhysRevA.81.022502 PACS number(s): 31.30.Gs

I. INTRODUCTION

Ions of the aluminum isoelectronic sequence have three valence electrons outside a closed $n = 2$ core and provide a model for studying the effects of strong correlations on closely spaced levels in heavy atoms. There are many examples in the Al sequence of level crossings of states having the same parity and angular momentum; such examples occur for both low and high values of the nuclear charge Z. Notably, the $3s3p^2$ and $3s^2 3p$ levels become relatively more tightly bound as the nuclear charge Z increases. Such crossings provide stringent tests of atomic structure calculations. Comparisons with measurements of fine-structure splitting energies, transition rates, line strengths, and fine-structure intervals also provide useful tests of the quality of different theoretical models. Many experimental energy levels and fine-structure intervals are now available up to very high nuclear charge ($Z = 40$) for $3s3p^2$ and $3s^2 3p$ levels; additionally, theoretical rates and line strengths for some transitions between these levels are available. The objective of this paper is to present a comprehensive set of calculations for $3s3p^2$ and $3s^2 3p$ energies to compare with previous calculations and experiments for the entire Al isoelectronic sequence. Most earlier measurements and calculations focused on $3s^2 3p$ states and low-lying $3s3p^2$ levels. Experimental measurements of a large number of energy levels are available (e.g., Kr XXIV and Mo XXX [1], Ca VIII–Zn XVIII [2], P III–Mo XXX [3], Ge XXX, Se XXII, Sr XXVI, Y XXVII, and Zr XXVII [4], Fe XIV [5,6], and Cu XVII–Mo XXX [7]). Experimental verifications should become simpler and more reliable using this more accurate set of calculations.

Two decades ago the theoretical situation for the Al-like $3s^2 3p$-$3s3p^2$ transitions lines was quite confusing. Many *ab initio* calculations using a wide range of different methods have also been done for calculating fine-structure energy levels and lifetimes. To mention just a few, fine-structure energy levels in Si II [8] and Al I–Fe XIV [9] have been calculated using the multiconfiguration Hartree–Fock (MCHF) approach, Cl V [10], Mn XIII [11], Co XV [12], Fe XIV, and Ni XVI [13] using CIV3, S IV [14] and Ar VI [15] using configuration-interaction (CI) expansions, P III–Mo XXX [16], Xe XXXXII [17], and Au LXVII [18] using the many-body perturbation theory (MBPT) approach, Ca VIII [19] using the R-matrix approximation, K VII [20] using the multiconfiguration Hartree-Dirac-Fock method (MCDHF) method, and Si II [21] using the relativistic quantum defect orbital (RQDO) method. Both experiment and theory have been used to investigate the fine structure for medium- to low-Z ions. Our calculations are motivated by the need for accurate fine-structure data in a variety of scientific applications, for improved understanding of the origin of these effects and for explanation of the existing results and making further predictions.

On the basis of our previous work [22,23], in this paper, besides the well-known problems arising from the necessity of considering some of the core electrons within the atom and the effects of electron correlation, relativity has to be taken into account in accurate calculations. The calculation methods used are based on the MCDHF method [24], as represented by the GRASP2K codes originating in Oxford [25] and further developed by Jönsson *et al.* [26]. It is a modification and extension of the GRASP92 codes by Parpia *et al.* [27]. As will be shown in the current work, the MCDHF (OL) mode, which has been applied successfully to a number of atomic systems and spectroscopic properties, is used to investigate the convergence of fine structure, transition rates, wavelengths, and line strengths in aluminum like ions ($26 \leqslant Z \leqslant 79$). The quality of the variational wave functions and the reliability of the calculated expectation values are assessed from the analysis of the convergence patterns as the approximate wave function is systematically improved, and from the comparison with the available theoretical and experimental data.

---

[*] gjiang@scu.edu.cn

The aim of the present paper is to extend our systematic approach to include new effects and to mainly concentrate on the low end of the sequence, where correlation effects are most important. We will investigate the importance of the core-valence correlation, which so far has rarely been included explicitly in any of the calculations for Al-like isoelectronic sequence. An important part of our approach is an attempt to define a method to estimate uncertainties in *ab initio* calculations and apply them to our calculations and, when possible, those of others.

II. THEORETICAL METHOD

The extended optimal level (EOL) version of the MCDHF method is used to calculate the transitions. The theoretical basis of our present computational approach has been widely discussed elsewhere [26–28]. In this paper, we give a brief overview of the salient features of the MCDHF model with configuration interaction.

In the MCDHF method, a configuration state function $\phi(\Gamma J^p)$ of a certain J and parity are formed by taking a linear combination of Slater determinants of the Dirac orbitals. A linear combination of these configuration state functions (CSFs) is then used in the construction of atomic state functions (ASFs) with the same J and parity:

$$\Psi_i(J^p) = \sum_{\alpha=i}^{n_{\text{csf}}} c_{i\alpha}\phi(\Gamma_\alpha J^p), \tag{1}$$

where $c_{i\alpha}$ are the mixing coefficients for the state i and n_{csf} is the number of CSFs included in the evaluation of the ASFs. The ASFs thus constructed are used in solving the Dirac–Hratree–Fock equation, and the Dirac–Coulomb Hamiltonian is

$$\hat{H}^{\text{DC}} = \sum_{i=1}^{N} \hat{H}_D(i) + \sum_{i=1}^{N-1}\sum_{j=i+1}^{N} |\hat{r_i} - \hat{r_j}|^{-1}, \tag{2}$$

where the first term, in *JJ* coupling, is the one-body contribution for an electron due to the kinetic energy and interaction with the nucleus. The two-body Coulomb interactions between the electrons comprise the second term. In the relativistic self-consistent field procedure both the radial parts of the Dirac orbitals and the expansion coefficients $c_{i\alpha}$ were optimized to self-consistency [29]. The contributions from the Breit interaction, vacuum polarization, self-energy, and finite nuclear mass corrections are not included in Eq. (2) and are generally added as a first-order perturbation correction after self-consistency is obtained. The transverse Breit interaction

$$B_{ij} = -\frac{1}{2r_{ij}}\left[\alpha_i \cdot \alpha_j + \frac{(\alpha_i \cdot r_{ij})(\alpha_j \cdot r_{ij})}{r_{ij}^2}\right] \tag{3}$$

was included in subsequent CI calculations [30].

III. GENERATION OF CONFIGURATION EXPANSIONS

In this work, we included different correlations into the calculation in a systematic approach. The correlation energy is defined as the energy difference between the exact solution to the Dirac equation and the Dirac-Fock (DF) solution. The contribution from different types of correlation can then be defined as the energy difference between the solution including the particular correlation under investigation and the DF solution. To classify the correlation, the atomic electrons can be divided into two parts: valence electrons and core electrons. As a result, the correlation between the valence electrons is defined as the valence correlation (VV), and the correlation between the valence electrons and core electrons is defined as the core-valence correlation (CV). The remaining correlation is the core-core correlation (CC), which describes the correlation between the core electrons. In the MCDHF approach, the correlation is represented by different constraints on the generation of the CSFs included in Eq. (1). If we only include the VV correlation, the core electrons are kept fixed in all the CSFs generated. To include the CV correlation, we allow one of the core electrons to be excited to generate the CSFs. Finally, the CC correlation can be taken into account by allowing more than one core electron to be excited.

It is, from some perspectives, desirable to perform separate calculations for each of the studied atomic states. This approach, however, is impractical and time consuming. Instead the atomic state functions for a number of closely spaced levels were determined together in the so-called EOL procedure. To account for the close degeneracy between $3s3p^2$ and $3s^23p$, the atomic state functions for $3s3p^2\,{}^2S_{1/2}$, $3s3p^2\,{}^4P_{1/2,3/2,5/2}$, $3s3p^2\,{}^2D_{3/2,5/2}$, and $3s^23p\,{}^2P_{1/2,3/2}$, were determined simultaneously. In the remaining cases atomic state functions for levels belonging to the same configuration were grouped together.

In our calculations, we generate the CSFs using the active space approach. We do this by exciting electrons from the spectroscopic reference configurations to a set of orbitals called the active set (AS). The active set is a set of orbitals which are all orbitals except those common to all CSFs, and it defines the CSFs included in the ASF. We increase the AS in a systematic way to ensure the convergence of the atomic parameters under consideration.

IV. COMPUTATIONAL DETAILS

As a starting point, MCDHF calculations in the EOL scheme were performed for each group of atomic states using configuration expansions including all lower states of the same J symmetry and parity, and we use a Dirac-Coulomb version, for the optimization of the orbitals, and include Breit corrections in a final configuration interaction calculation. To build a CSF expansion, restrictive active space methods were used. The idea of active space methods is to consider only electrons from the active space and to excite them from the occupied orbitals to unoccupied ones. The orbital was increased systematically in order to monitor the convergence of the calculation. Since the orbitals with the same principal quantum number n often have similar energies, the active set is usually enlarged in steps of orbital layers. It is convenient to refer to the $\{1s, 2s, 2p, 3s, 3p, 3d\}$ set of orbitals as the $n = 3$ orbital layer, $\{1s, 2s, 2p, \ldots, 4s, 4p, 4d, 4f\}$ as the $n = 4$ layer, etc. Larger orbital sets can result in a considerable increase of computational time required for the problem, and appropriate restrictions may be necessary. We divided the calculations into two parts, one where we optimized a set of orbitals for the even states and one for the odd states (i.e., the upper and lower states were described by two independently optimized sets of orbitals). Because of this we had to use a biorthogonal transformation [28] of the atomic state functions to calculate the transition parameters.

A model including only the valence correlation will follow the constraint of closed-core subshells for all CSFs; that is, they will have the form

$$1s^2 2s^2 2p^6 n_1 l_1 n_2 l_2 n_3 l_3 \text{ (VV model)}.$$

To extend the model also to include the core-valence correlation, we relax the constraint to be

$$1s^2 2s^2 2p^5 n_1 l_1 n_2 l_2 n_3 l_3 n_4 l_4 \text{ (CV model)}.$$

To treat the core-core correlation in aluminum-like ions, we include all CSFs of the form

$$1s^2 2s^2 2p^4 n_1 l_1 n_2 l_2 n_3 l_3 n_4 l_4 n_5 l_5 \text{ (CC model)}.$$

An approach with no further constraints would represent the restricted active space for core-valence correlation with the $2p$ subshell (CV_{2p}). This kind of approach is feasible for simple systems, such as helium-like copper ions [31], with few valence electrons, But for the more complex aluminum like ions we need to use further constraints, defined by using a distribution strings of the type

$$\{n_1, n_2, \ldots\}^q.$$

This represents all possible distributions of q electrons among the shells specified by their principal quantum numbers $(n_1, n_2, \ldots)$ This VV model could be written as

$$1s^2 2s^2 2p^6 \{3\}^1 \{3, 4, 5, 6\}^2 \tag{4}$$

if we include orbitals with $n \leqslant 6$.

The EOL scheme used in this work includes several levels in the energy functional that takes into account the weights for the levels under consideration. In this method, the radial orbitals and the mixing coefficients are determined by optimizing the energy functional which is the weighted sum of the energy values corresponding to a set of eigenstates. The succeeding terms were then obtained by configuration mixing using an active space approximation. In the active space method, the *jj*-coupled CSFs of a given parity P and symmetry J are generated by excitations from the reference configuration to the active set of orbitals. Because the angular correlation is known to play an important role in relativistic calculations, in this work, the active set comprised all the orbitals up to $n = 6$ and $l = 3$. Single and double (SD) excitations of electrons were used to compute the correlation corrections to the energies and dipole rates. The virtual set was varied in a systematic way by increasing the principal quantum number n by one without imposing restrictions on the orbital quantum number. Our earlier calculations [23] indicate that the set that could be handled without any difficulty was up to $n = 6$. Also, for configurations with more than ten electrons, the number of CSFs generated was very large for double excitation and we could not carry out our relativistic configuration interaction (RCI) calculations due to storage limitations. In such cases, we restricted our calculations to single excitation but increased our active set up to $n = 7$. The initial and final orbital wave functions were generated by simultaneously optimizing them. Though this procedure was followed in this work to reduce the computational effort, it is found to yield quite accurate results. The optimized zero-order wave functions obtained using the reference configurations were used as a starting point for further MCDHF calculations. Once the convergence of the energy eigenvalues was obtained, the orbital basis from the MCDHF procedure was used to carry out the configuration interaction calculations.

A. Computational procedure

We perform a number of different sets of MCDHF calculations to investigate the importance of different effects. However, larger orbital sets can result in a considerable increase the of computational time required for the problem, and appropriate restrictions may be necessary.

In the first set of calculations, we only included valence correlations, by keeping the core $1s^2 2s^2 2p^6$ closed and common to all calculations. We start by optimizing all orbitals on the full active space of valence correlation CSFs:

$$2p^6 \{3\}^3, \quad J^\pi \in \{0^o, 1^o, 1^e, 2^o\}. \tag{5}$$

When deriving the specific form of MCDHF equations to solve, we start by applying the variational principle to a functional of energies. It is common to use an EOL technique, where a linear combination of the most important energy levels is used. However, it is important to remember that, especially for lower Z, the two configurations $3s3p4s$ and $3s3p3d$ are also important. This justifies our choice of optimization for $n = 4$:

$$2p^6 \{3\}^1 \{3, 4\}^2, \quad J^\pi \in \{0^o, 1^o, 1^e, 2^o\}. \tag{6}$$

For the $n = 4$ orbitals, we again use a complete VV space approach. First we add $4s$ and $4p$ to our active set and optimize these two orbitals on $3s3p4s\ {}^2P$. Then we also add $4d$ and $4f$ and optimize these two orbitals on the $3s3p3d\ {}^2P$ term.

This crosswise optimization technique gives a very flexible basis set, able to represent the quite large difference in $3s$ and $3p$ orbitals in the CSFs with only one 3s ($3s3p^2$) and the ones with a closed $3s$ subshell ($3s^2 3p$ and $3s^2 nl$).

In two final calculations we add $n = 5$ and 6 (with $l \leqslant 3$) orbitals to the active set. To generate CSFs we used single and double replacements from the multireference set $3s^2 3p$, $3s3p3d$, $3s3p4s$ for the odds and only $3s3p^2$ for the evens. The new orbitals were optimized on the lowest ${}^2P^o$ and ${}^2P^e$ terms separately. Where we generated all CSFs of the form

$$2p^6 \{3\}^1 \{3, 4, 5\}^2, \quad J^\pi \in \{0^o, 1^o, 1^e, 2^o\}, \tag{7}$$

and

$$2p^6 \{3\}^1 \{3, 4, 5, 6\}^2, \quad J^\pi \in \{0^o, 1^o, 1^e, 2^o\}. \tag{8}$$

To investigate the convergence we found it necessary to add another layer in a slightly different way. We generated a configuration list from

$$2p^6 \{3\}^1 \{3, 4, 5, 6, 7s, 7p, 7d\}^2, \quad J^\pi \in \{0^o, 1^o, 1^e, 2^o\}, \tag{9}$$

but kept only those CSFs which could interact with the reference configurations in first order and added these to the CSFs from the last step. This was then followed by a CI calculation where all configurations were included.

TABLE I. Aluminum-like isoelectronic sequence: excitation energies (in cm^{-1}) from MCDHF calculations and experiment.

		MCDHF								
		VV			CV			CC		
Level		$n \leqslant 4$	$n \leqslant 5$	$n \leqslant 6$	$n \leqslant 7$	$n \leqslant 5$	$n \leqslant 6$	$n \leqslant 3$	$n \leqslant 4$	Expt. [34]
$Z = 26$ Fe XIV										
$3s^23p$	${}^2P_{1/2}$	0	0	0	0	0	0	0	0	0
	${}^2P_{3/2}$	18 778	18 773	18 773	18 773	18 866	18 834	18 845	18 858	18 852.5
$3s3p^2$	${}^4P_{1/2}$	223 599	223 868	223 908	223 923	224 482	224 452	223 384	222 155	225 114
	${}^4P_{3/2}$	231 228	231 498	231 539	231 555	232 153	232 112	231 009	229 780	232 789
	${}^4P_{5/2}$	240 837	241 099	241 139	241 155	241 794	241 732	240 669	239 465	242 387
	${}^2D_{3/2}$	299 648	299 718	299 695	299 689	300 662	300 636	301 031	301 694	299 242
	${}^2D_{5/2}$	301 828	301 898	301 875	301 870	302 903	302 866	303 413	303 826	301 469
	${}^2S_{1/2}$	367 870	367 531	367 458	367 439	367 156	366 529	370 108	369 992	364 693
	${}^2P_{1/2}$	393 121	392 893	392 859	392 842	390 792	390 262	391 106	391 959	388 510
	${}^2P_{3/2}$	401 586	401 387	401 363	401 347	398 717	398 239	402 150	402 082	396 512
$Z = 36$ Kr XXIV										
$3s^23p$	${}^2P_{1/2}$	0	0	0	0	0	0	0	0	0
	${}^2P_{3/2}$	97 160	97 173	97 175	97 176	97 353	97 337	97 240	97 383	97 312
$3s3p^2$	${}^4P_{1/2}$	410 788	411 046	411 084	411 101	411 569	411 668	410 944	409 767	411 750
	${}^4P_{3/2}$	462 535	462 844	462 894	462 914	463 526	463 662	462 547	461 513	464 204
	${}^4P_{5/2}$	499 288	499 555	499 595	499 611	500 242	500 343	499 574	498 988	500 424
	${}^2D_{3/2}$	580 654	580 749	580 725	580 723	581 511	581 641	582 018	583 361	579 808
	${}^2D_{5/2}$	611 809	611 956	611 941	611 943	613 044	613 202	613 143	614 144	611 662
	${}^2P_{1/2}$	662 731	662 518	662 466	662 450	660 389	659 952	663 791	661 265	657 825
	${}^2S_{1/2}$	759 024	758 769	758 700	758 680	757 560	757 024	760 784	758 454	754 727
	${}^2P_{3/2}$	770 940	770 794	770 753	770 740	767 964	767 697	771 470	771 076	765 062
$Z = 42$ Mo XXX										
$3s^23p$	${}^2P_{1/2}$	0	0	0	0	0	0	0	0	0
	${}^2P_{3/2}$	203 816	203 837	203 844	203 845	204 094	204 106	203 877	204 145	204 020
$3s3p^2$	${}^4P_{1/2}$	539 341	539 547	539 667	539 590	539 961	540 083	539 744	538 502	538 435
	${}^4P_{3/2}$	667 097	667 406	667 525	667 489	668 162	668 428	667 182	666 309	
	${}^4P_{5/2}$	723 405	723 636	723 755	723 690	724 346	724 546	723 987	723 968	
	${}^2D_{3/2}$	818 064	818 139	818 259	818 134	818 815	819 074	819 456	820 177	816 860
	${}^2D_{5/2}$	914 023	914 220	914 339	914 235	915 629	916 047	915 152	916 377	914 330
	${}^2P_{1/2}$	896 434	896 280	896 399	896 222	893 745	893 363	894 133	894 467	891 280
	${}^2S_{1/2}$	11 00 264	11 00 021	11 00 140	10 99 923	10 99 216	10 98 614	11 02 239	11 02 101	10 95 240
	${}^2P_{3/2}$	11 17 839	11 18 056	11 18 184	11 18 080	11 16 922	11 17 153	11 18 229	11 18 153	11 50 820

After this the results seemed to have converged, and these results are still a satisfactory representation of the valence correlation.

In spite of the fact that the valence correlation approach seemed to converge, there were signs of significant uncertainties. For Fe XIV, the computed (392 842 cm^{-1}) fine structure of the excitation term deviated clearly from the experimental value (388 510 cm^{-1}) (see Table I). The same was true for the term splitting between ${}^4P$ and ${}^2P$, which was off by about 0.5%–1.2%. Comparison with known energy differences is one of our most important tools for determining uncertainties in the calculations, so we concluded that our VV calculations were associated with large uncertainties (up to 2.8%, as we will see in the following). The reason was interpreted as a systematic error, resulting from a left-out correlation.

To include more correlations, we define a core–valence approach. For the core–valence correlations, we instead used all CSFs from the second step and added all CSFs of the form

$$2p^5\{2,3\}^2\{3,4\}^1\{3,4,5\}^1, \quad J^\pi \in \{0^o, 1^o, 1^e, 2^o\}, \tag{10}$$

with $l \leqslant 3$, and optimized the $n = 5$ orbitals to account for the effect of polarization of the $2p$ core. In this way, the core–valence correlation between the $2p$ shell and the valence shell was included. In the final calculation, we included all CSFs from the last step and added all CSFs

$$2p^6\{3,4\}^2\{3,4,5,6s,6p,6d\}^1, \quad J^\pi \in \{0^o, 1^o, 1^e, 2^o\}, \tag{11}$$

with $l \leqslant 3$, and optimized the orbitals $n = 5f$, $6s$, $6p$, and $6d$. Our RCI expansions include up to 45 239 CSFs for the ground state and 59 513 CSFs for the excited states based on SD excitations from the reference configurations. Contributions from higher partial waves with $l > 3$ are small and are obtained by extrapolations.

To investigate the effect of the core–core correlation, we opened the $2s2p$ shell for double substitutions to the $n = 3$ layer and added these new configurations to the final core-valence expansion. Then, we opened the $1s$ shell for double substitutions to the $n = 4$ layer and we found that this shell contributed less than 0.8% to the energies value. In order to reduce the amount of numerical calculation, our final core-core correlation of the aluminum isoelectronic sequence only included the substitution from the core $2s2p$ to the $n = 3$ layer. For the aluminum isoelectronic sequence, the final core-core correlation is based on the calculation of expansions over the set of configuration states

$$\{1\}^2\{2\}^6\{3\}^5, \quad J^\pi \in \{0^o, 1^o, 1^e, 2^o\}. \tag{12}$$

In these three models, the energy contributions from the Breit interaction, quantum electrodynamics (QED) corrections, and the specific mass shift (SMS) were included. The mixing coefficients obtained using MCDHF and RCI orbital wave functions in the block structure format were then converted into nonblock format and the orbital wave functions of the initial and final states were transformed to a new representation in which the two orbitals are biorthonormal [28,32]. These biorthonormal wave functions were used in the evaluation of the dipole transition rates. In this implementation of the RCI program an iterative Davidson method was used together with a spare matrix representation allowing for large expansions.

B. Uncertainty estimates

We consider it important to not only present results for the intercombination lines but also to make an attempt to estimate the uncertainties of these results. As we proceed through our calculations we try to follow a set of quality criteria which highlight the accuracy of the results and aid in determining uncertainty estimates. We look at the following:

(i) Convergence of systematic calculations—the process of systematic calculations includes the optimization of orbitals, their inclusion in the orbital set, and the manner in which we generate CSFs. As the calculations evolve these systematics emphasize the convergence of results.

(ii) Results for known properties—experimental energy spectra give us a set of known properties, which are useful as an accuracy gauge as the calculations proceed.

(iii) Theoretical tests—agreement between the length and velocity forms of transition line strengths for allowed lines also provides a means of gauging the accuracy of a calculation and contributes to the uncertainty of the calculation. We note that exact agreement between length and velocity is a necessary but not a sufficient condition.

Our approach is not aimed at being based on a strong theoretical argument, but rather on a reasonable first-order model. If we assume that the intercombination line is induced by mixing with a $^2P^o$, then perturbation theory gives

$$S_{\rm sf} \approx \left(\frac{\langle ^2P^o_{1/2}|H|^2S_{1/2}\rangle}{E_T}\right)^2 S_A, \tag{13}$$

where $S_{\rm sf}$ is the "spin-forbidden" line strength, S_A is the line strength for the allowed $^2P^o$–$^2P^o$ transition, and $\langle ^2P^o_{1/2}|H|^2S_{1/2}\rangle$ is the off-diagonal matrix element between $3s3p^2\,{}^2P^o_{1/2}$ and $^2S_{1/2}$. E_T is the term splitting:

$$E_T = E(3s3p^2\,{}^2P_{1/2}) - E(3s3p^2\,{}^2S_{1/2}). \tag{14}$$

Because the electric dipole operator H does not involve spin coordinates, the matrix element calculation is simplest in LS-coupled bases. The only contribution to $\langle ^2P^o_{1/2}|H|^2S_{1/2}\rangle$ comes from operators that are not diagonal in the total spin, which are spin-dependent operators. The same operators also give the fine structures of different terms. Therefore, it is fair to assume that the uncertainty in the off-diagonal element is equal to the uncertainty in the fine structure of a given term:

$$\delta\langle ^2P^o|H|^2S\rangle \approx \delta E_{\rm fs}. \tag{15}$$

Taking note of the delta factor in (15) and of the triangle relations that must be satisfied for the 6-j symbol to be nonzero. This, together with Eq. (13), supplies us with a means of estimating the uncertainty in $S_{\rm sf}$ according to

$$\delta S_{\rm sf} \approx 2\delta E_{\rm fs} + 2\delta E_T + \delta S_A, \tag{16}$$

where δ denotes the uncertainty. The last term, the uncertainty in the allowed line strength, is usually negligible compared to the two other contributions. The uncertainty in the computed transition rate, $A_{\rm sf}$, or lifetime, τ, is the same as in the line strength, if we use experimental transition energies.

We now define the uncertainty in a computed energy property as

$$\delta E_x = |\Delta x - 1|, \quad \text{where} \quad \Delta x = \frac{E_x(\text{experiment})}{E_x(\text{theory})} \tag{17}$$

(x = fs or T). Also, the line strength contribution is given by

$$\delta S_A = |\Delta_A - 1|, \quad \text{where} \quad \Delta_A = \frac{S_l}{S_v}. \tag{18}$$

For the fine-structure splitting we chose the $3s^23p\,{}^2P^o$ ground term over the $3s3p^2\,{}^2P$ term because the splitting of the latter is zero in first order.

Not only are the aluminum-like $3s3p^2\,{}^2S_{1/2}$–$3s^23p\,{}^2P^o_{1/2,3/2}$ [$E1$] lines, in combination with other transitions, important in electron temperature and density diagnostics but the relative intensity of these two transitions provides a good indication of the optical depth of the source, since they originate from the same upper level. Since both the lifetime and the branching ratio are directly measurable, with very few assumptions for the observed plasma, they are also excellent test cases for atomic theoretical models and experimental methods.

The theory provides us with computed transition rates

$$A_1 = A(3s3p^2\,{}^2S_{1/2} - 3s^23p\,{}^2P^o_{1/2})$$

and

$$A_2 = A(3s3p^2\,{}^2S_{1/2} - 3s^23p\,{}^2P^o_{3/2}), \tag{19}$$

while the measurable and, for diagnostics, interesting properties are the branching ratio

$$Q = \frac{A_2}{A_1} \tag{20}$$

and the lifetime

$$\tau = \frac{1}{A_1 + A_2}. \tag{21}$$

In Table II we show the uncertainties we have outlined here for the final valence correlation and core-valence and core-core correlation calculations of MCDHF, compared with

TABLE II. Derived uncertainties and contributions to *ab initio* $[E1]A$ values. Numbers in square brackets denote powers of 10.

	MCDHF ($Z = 26$)				MCDHF ($Z = 28$)			
Property	VV $n \leqslant 7$	CV $n \leqslant 6$	CC $n \leqslant 3$	Expt.[a]	VV $n \leqslant 7$	CV $n \leqslant 6$	CC $n \leqslant 3$	Expt.[b]
S_l/S_v	2.49[−1]/ 2.54[−1]	2.09[−1]/ 2.00[−1]	2.24[−1]/ 2.25[−1]		1.47[−1]/ 1.50[−1]	1.21[−1]/ 1.15[−1]	1.29[−1]/ 1.30[−1]	
δS_A	1.97[−2]	4.50[−2]	4.44[−3]		1.80[−2]	5.22[−2]	7.69[−3]	
E_T	25404	23733	23998	23832	31731	30622	30826	30720
δE_T	6.19[−2]	4.17[−3]	6.92[−3]		3.19[−2]	3.20[−3]	3.44[−3]	
E_{fs}	18773	18835	18845	18852	27665	27744	27739	27760
δE_{fs}	4.21[−3]	9.03[−4]	3.71[−4]		3.43[−3]	5.77[−4]	7.57[−4]	
Percentage uncertainties								
δS_A	1.97%	4.50%	0.44%		1.80%	5.22%	0.77%	
$2 \times \delta E_T$	12.38%	0.83%	1.38%		6.38%	0.64%	0.69%	
$2 \times \delta E_{\text{fs}}$	0.84%	0.18%	0.07%		0.69%	0.12%	0.15%	
Total δA_{sf}	15.19%	5.51%	1.89%		8.87%	5.98%	1.61%	

	MCDHF ($Z = 34$)				MCDHF ($Z = 36$)			
Property	VV $n \leqslant 7$	CV $n \leqslant 6$	CC $n \leqslant 3$	Expt.[c]	VV $n \leqslant 7$	CV $n \leqslant 6$	CC $n \leqslant 3$	Expt.[d]
S_l/S_v	2.82[−2]/ 2.86[−2]	2.37[−2]/ 2.24[−2]	2.52[−2]/ 2.72[−2]		1.68[−2]/ 1.70[−2]	1.44[−2]/ 1.36[−2]	1.52[−2]/ 1.63[−2]	
δS_A	1.40[−2]	5.80[−2]	7.35[−2]		1.18[−2]	5.88[−2]	6.75[−2]	
E_T	72935	73381	73389	74308	96231	97072	96993	96902
δE_T	1.88[−2]	1.26[−2]	1.25[−2]		6.97[−3]	1.75[−3]	9.38[−4]	
E_{fs}	73485	73631	73556	73626	97176	97337	97241	97312
δE_{fs}	1.92[−3]	6.79[−5]	9.52[−4]		1.40[−3]	2.57[−4]	7.30[−4]	
Percentage uncertainties								
δS_A	1.40%	5.80%	7.35%		1.18%	5.88%	6.75%	
$2 \times \delta E_T$	3.76%	2.52%	2.50%		1.39%	0.35%	0.19%	
$2 \times \delta E_{\text{fs}}$	0.39%	0.01%	0.19%		0.28%	0.05%	0.15%	
Total δA_{sf}	5.52%	8.33%	10.04%		2.85%	6.28%	7.09%	

	MCDHF ($Z = 40$)				MCDHF ($Z = 42$)			
Property	VV $n \leqslant 7$	CV $n \leqslant 6$	CC $n \leqslant 3$	Expt.[c]	VV $n \leqslant 7$	CV $n \leqslant 6$	CC $n \leqslant 3$	Expt.[d]
S_l/S_v	6.42[−3]/ 6.48[−3]	5.68[−3]/ 5.89[−3]	5.96[−3]/ 6.47[−3]		4.09[−3]/ 4.11[−3]	3.69[−3]/ 3.46[−3]	3.84[−3]/ 4.26[−3]	
δS_A	9.26[−3]	3.57[−2]	7.88[−2]		4.87[−3]	6.65[−2]	9.86[−2]	
E_T	160887	162299	162110	161617	205987	202635	205115	203960
δE_T	4.54[−3]	4.20[−3]	3.04[−3]		9.84[−4]	6.54[−3]	5.63[−3]	
E_{fs}	161511	161734	161654	161680	203845	204106	203877	204020
δE_{fs}	1.05[−3]	3.34[−4]	1.61[−4]		8.58[−4]	4.21[−4]	7.01[−4]	
Percentage uncertainties								
δS_A	0.93%	3.57%	7.88%		0.49%	6.65%	9.86%	
$2 \times \delta E_T$	0.91%	0.84%	0.61%		0.20%	1.31%	1.13%	
$2 \times \delta E_{\text{fs}}$	0.21%	0.07%	0.03%		0.17%	0.08%	0.14%	
Total δA_{sf}	2.05%	4.48%	8.52%		0.86%	8.04%	11.13%	

[a] Redfors and Litzen [5].

[b] Bhatia and Doschek [33].

[c] Ekberg and Redfors [4].

[d] Sugar and Kaufman [7].

experimental results. We note that we use the $3s^23p\ ^2P_{1/2}$–$3s3p^2\ ^2P_{1/2}$ S values to estimate δS_A in MCDHF calculations.

V. RESULTS AND DISCUSSION

While considering the convergence and accuracy of our calculation and comparing the three interactions (i.e., VV, CV, and CC), we monitored the VV, CV, and CC forms of the MCDHF and RCI excitation energies in Fe XIV, Kr XXIV, and Mo XXX for orbital sets of increasing size, denoted by n. In Table I, It is obvious that, although the excitation energy of the $3s3p^2\ ^2D^e$ level in the valence correlation $n \leqslant 4$ calculation agrees reasonably well with the experiment, this is not true for the other levels. Many of the calculated levels in the valence correlation $n \leqslant 5$ calculation appear to be

TABLE III. *LSJ* line strengths [S_l/S_v]. Numbers in square brackets denote powers of 10.

Transition	CV $n \leqslant 3$	CV $n \leqslant 4$	CV $n \leqslant 5$	CV $n \leqslant 6$
		$Z = 26$ Fe XIV		
$3s3p^2\,{}^4P_{3/2}$–$3s^23p\,{}^2P_{1/2}$	6.44[−5]/6.53[−5]	6.45[−5]/6.55[−5]	6.50[−5]/6.58[−5]	6.52[−5]/6.59[−5]
–$3s^23p\,{}^2P_{3/2}$	1.20[−3]/1.23[−3]	1.21[−3]/1.22[−3]	1.22[−3]/1.22[−3]	1.21[−3]/1.21[−3]
$3s3p^2\,{}^2P_{1/2}$–$3s^23p\,{}^2P_{1/2}$	2.52[−1]/2.42[−1]	2.53[−1]/2.46[−1]	2.54[−1]/2.48[−1]	2.54[−1]/2.49[−1]
–$3s^23p\,{}^2P_{3/2}$	4.22[−1]/4.10[−1]	4.23[−1]/4.11[−1]	4.24[−1]/4.13[−1]	4.24[−1]/4.13[−1]
		$Z = 36$ Kr XXIV		
$3s3p^2\,{}^4P_{3/2}$–$3s^23p\,{}^2P_{1/2}$	2.60[−4]/2.78[−4]	2.61[−4]/2.77[−4]	2.61[−4]/2.76[−4]	2.61[−4]/2.76[−4]
–$3s^23p\,{}^2P_{3/2}$	3.37[−3]/3.45[−3]	3.38[−3]/3.44[−3]	3.37[−3]/3.43[−3]	3.37[−3]/3.42[−3]
$3s3p^2\,{}^2P_{1/2}$–$3s^23p\,{}^2P_{1/2}$	1.73[−2]/1.66[−2]	1.70[−2]/1.68[−2]	1.70[−2]/1.68[−2]	1.70[−2]/1.68[−2]
–$3s^23p\,{}^2P_{3/2}$	1.86[−1]/1.76[−1]	1.87[−1]/1.78[−1]	1.88[−1]/1.79[−1]	1.88[−1]/1.80[−1]
		$Z = 42$ Mo XXX		
$3s3p^2\,{}^4P_{3/2}$–$3s^23p\,{}^2P_{1/2}$	3.63[−4]/3.75[−4]	3.64[−4]/3.79[−4]	3.64[−4]/3.80[−4]	3.64[−4]/3.80[−4]
–$3s^23p\,{}^2P_{3/2}$	4.33[−3]/4.42[−3]	4.35[−3]/4.42[−3]	4.36[−3]/4.41[−3]	4.36[−3]/4.40[−3]
$3s3p^2\,{}^2P_{1/2}$–$3s^23p\,{}^2P_{1/2}$	1.51[−1]/1.55[−1]	1.52[−1]/1.54[−1]	1.51[−1]/1.53[−1]	1.51[−1]/1.52[−1]
–$3s^23p\,{}^2P_{3/2}$	1.32[−2]/1.24[−2]	1.29[−2]/1.26[−2]	1.29[−2]/1.26[−2]	1.30[−2]/1.26[−2]
		$Z = 54$ Xe XXXXII		
$3s3p^2\,{}^4P_{3/2}$–$3s^23p\,{}^2P_{1/2}$	4.49[−4]/4.58[−4]	4.51[−4]/4.61[−4]	4.50[−4]/4.62[−4]	4.50[−4]/4.62[−4]
–$3s^23p\,{}^2P_{3/2}$	4.58[−3]/4.90[−3]	4.60[−3]/4.91[−3]	4.61[−3]/4.91[−3]	4.61[−3]/4.90[−3]
$3s3p^2\,{}^2P_{1/2}$–$3s^23p\,{}^2P_{1/2}$	7.40[−2]/7.48[−2]	7.41[−2]/7.47[−2]	7.43[−2]/7.46[−2]	1.56[−2]/1.44[−2]
–$3s^23p\,{}^2P_{3/2}$	1.56[−2]/1.42[−2]	1.55[−2]/1.43[−2]	1.56[−2]/1.43[−2]	1.56[−2]/1.44[−2]
		$Z = 79$ Au LXVII		
$3s3p^2\,{}^4P_{3/2}$–$3s^23p\,{}^2P_{1/2}$	3.15[−4]/3.12[−4]	3.16[−4]/3.14[−4]	3.16[−4]/3.15[−4]	3.16[−4]/3.17[−4]
–$3s^23p\,{}^2P_{3/2}$	2.55[−3]/2.92[−3]	2.56[−3]/2.91[−3]	2.57[−3]/2.91[−3]	2.57[−3]/2.90[−3]
$3s3p^2\,{}^2P_{1/2}$–$3s^23p\,{}^2P_{1/2}$	2.62[−2]/2.68[−2]	2.63[−2]/2.65[−2]	2.63[−2]/2.65[−2]	2.61[−2]/2.65[−2]
–$3s^23p\,{}^2P_{3/2}$	8.29[−3]/8.12[−3]	8.30[−3]/8.14[−3]	8.32[−3]/8.15[−3]	8.32[−3]/8.16[−3]

in reasonable agreement with the experiment; however, it is necessary to increase the orbital set further to represent the states to a similar extent and to induce stability in the ground state. Comparing the valence correlation and core–valence correlation $n \leqslant 5$ calculations we see that adding in these additional CSFs has pushed the ground state down except for the $3s3p^2\,{}^2P^e_j$ and ${}^2S^e_{1/2}$ levels, but the more important term splitting (the energy difference between different *LS* terms) actually improves slightly. Although the $6d$ orbital was specifically optimized to represent core polarization effects it has little effect on the excitation energies. It seems that the most important core effects have already been included. However, we shall keep this orbital in our calculations to be consistent with the effects it represents. We have only given the core–core correlation $n \leqslant 4$ results, but, as we see from Table I, adding in the $4d$ has had a negligible effect on the energies of the system and will, therefore, be neglected in further calculations.

In Table III, we present values of line strengths calculated in length S_l and velocity S_v forms for the two $E1$ lines. The results are from the various core-valence correlation calculations. The convergence of the results is clearly seen as n increases in the core-valence correlation calculations. As can be seen from this table, the agreement of the two gauges is very good and the near-equal values of the length and velocity of the transitions give an additional check on the accuracy of our results. And the agreement of the two gauges improves with increasing n. At the same time, we can find that the length value is more stable in that it changes less as the active space extends. And, for this reason, we use length gauge in our present work. We would put an accuracy of about 5% on these allowed transition S values, although in many cases the accuracy is much better than this.

The core-valence correlation effect, measured by the difference among the MCDHF_VV, MCDHF_CV and MCDHF_CC calculations, is more interesting. A number of different energies would be interesting to monitor and compare with experiment. First, in Table IV, we compare results for the four fine-structure intervals $3s^23p$ [${}^2P^2_{3/2}$–$P_{1/2}$], $3s3p^2$ [${}^4P^4_{3/2}$–$P_{1/2}$], $3s3p^2$ [${}^2D_{5/2}$–${}^2D_{3/2}$], and $3s3p^2$ [${}^4P^4_{5/2}$–$P_{3/2}$] in aluminum-like ions with $Z = 26$ to 42. Our MCDHF values are compared with predicted data given by Safronova *et al.* [16], given by Ekberg and Redfors [4], and as recommended by the National Institute of Standard and Technology (NIST) presented in [34]. The mixing among some of the relativistic levels is found to be very strong. To keep our *ab initio* energies as close as possible to the experimental values, we have made small J-dependent adjustments to the diagonal elements of the Hamiltonian matrices. These adjustments improve the accuracy of the mixing $c_{i\alpha}$ coefficients, which depend in part on the accuracy of the eigenvalues. This is a justifiable [35] fine-tuning technique and is particularly useful for the calculation of intercombination lines. These adjustments also affect the composition of the eigenvectors slightly. In a way, we correct the ab *initio* approach for the neglected core–valence correlation, which has been shown to contribute significantly in neutral magnesium (see, for instance, Ref. [36]). From Table IV it is clear that including the CV correlation does affect the energy spectrum substantially for Fe XIV–Mo XXX. This is

TABLE IV. Comparison of present fine-structure splitting values (in cm^{-1}) of some $3s^23p$ and $3s3p^2$ levels with experimental results and calculations of Safronova *et al.* (MBPT). The values are for the $n = 6$ (VV correlation), $n = 6$ (CV correlation), and $n = 3$ (CC correlation) active sets corrected for the core–valence electrons interactions.

	$3s^23p[^2P_{3/2}–^2P_{1/2}]$					$3s3p^2[^4P_{3/2}–^4P_{1/2}]$				
Z	VV	CV	CC	Expt.[a]	MBPT[b]	VV	CV	CC	Expt[a]	MBPT[b]
26	18773	18835	18858	18852.5	18831	7632	7660	7624	7675	7702
28	27665	27744	27771	27760.4	27731	11795	11836	11779	11852	11899
34	73485	73631	73665	73626[c]	73555	36987	37198	36936	37243[c]	37244
36	97176	97337	97383	97312	97281	51813	51994	51746	52454	52190
40	161511	161734	161780	161680[c]	161599	96248	97573	96162	97257[c]	96858
42	203845	204106	204145	204020	203906	127899	128346	127806		128628
	$3s3p^2[^4P^4_{5/2}–P_{3/2}]$					$3s3p^2\ [^2D_{5/2}–^2D_{3/2}]$				
26	9600	9620	9686	9598	9562	2181	2230	2132	2227	
28	13623	13643	13770	13608	13545	4046	41112	3929	4153	
34	30213	30192	30773	30056[c]	29891	19921	20158	19900		
36	36697	36681	37027	36220	36255	31220	31562	31125	31854	
40	49826	49773	50339	49462[c]	49098	68403	69047	68119		
42	56201	56591	56805		55340	94444	95339	95469	97470	

[a] Taken from [34].
[b] Safronova *et al.* [16].
[c] Ekberg and Redfors [4].

true for the excitation energies and term splitting, but the most dramatic effect is on the fine structure. If we look at the three "pure" terms, the ground $3s^23p\,^2P$ and $3s3p^2\,^4P$, we see that in three cases the CV correlation results show excellent agreement with the experimental values of Ekberg and Redfors [4] to within a few percent (0.4% and 0.004%). Also, our calculations are also generally in good agreement with the MBPT results of Safronova *et al.* [16] and NIST data from [34] for low-Z ions. However, a more detailed comparison of the calculated and observed energies for these transitions (Table IV) indicates that some splitting energies given by Safronova *et al.* [16] calculations are in better agreement with NIST data than our GRASP2K results. This may be because we have included a limited number of configurations in our calculation. In the work presented here we have increased the number of configurations included or the size of the orbital set in a systematic manner until good convergence was obtained. This difference in the two methods should account for a large fraction of the disagreement in the results.

Our results primarily confirm previous data for Fe XIV, Ni XVI, Se XXII, Zr XXVII, Kr XXIV, Mo XXX, Xe XXXXII, and Au LXVII. However, the observation of intercombination lines of the $3s^23p\,^2P$–$3s3p^2\,^4P$ multiplet also provides new information about the quartet system. The isoelectronic trend of the wave numbers is shown in Fig. 1, where several intercombination lines have been observed by Träbert and co-workers [38,39] by means of time-delayed beam-foil spectroscopy for a number of ions from Ar VI to Zn XVIII. Relativity, however, changes the compositions of the levels as well as the relative amount of fine structure and electrostatic energy intervals (see Fig. 2 for an illustration of the level scheme). Consequently, the lines of the multiplet move apart on the wavelength scale, and the relative line intensities change. Near $Z = 79$ (Au), this short-wavelength branch outweighs the other by about a factor of 10 in transition probability [40]. Because of the quantum mechanical peculiarity of a matrix element, the upper level of this line, $^4P_{3/2}$, is much longer lived than the other two levels of the same term at low Z [31,32]. At high Z, however, the $^4P_{5/2}$ level is the longest lived [41]. One multiplet component, the $J = 3/2$ to $J' = 1/2$ line, even vanishes when the level sequence changes, that is, when the ground-state fine-structure interval grows larger than the $3s$-$3p$ energy difference (near $Z = 58$ [41]). Then the upper level ($J = 3/2$) of the $3s^23p^2P^o$ ground term crosses the position of the $J' = 1/2$ level of the excited (displaced) term $3s3p^2\,^4P$, and thereafter it lies higher in excitation energy. As a consequence of this, the energy-level pattern in the multiplet varies substantially. Also, it has been found that the calculated wave number data (in Fig. 1) seemed to follow a smooth trend

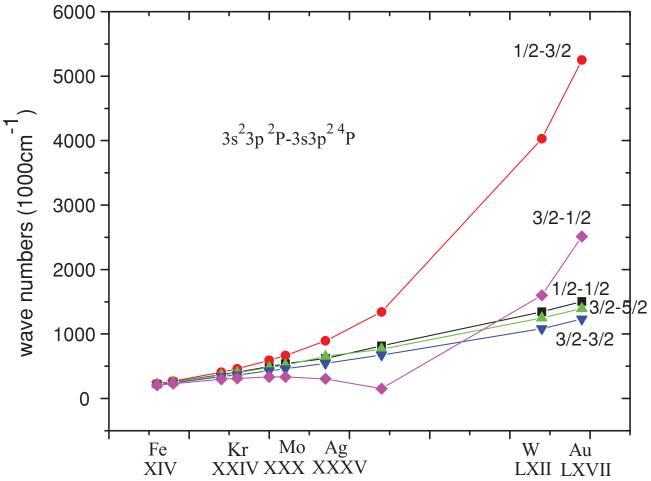

FIG. 1. (Color online) Isoelectronic evolution of the wave numbers of the spin-forbidden $3s^23p\,^2P$–$3s3p^2\,^4P$ transition in Fe XIV–Au LXVII.

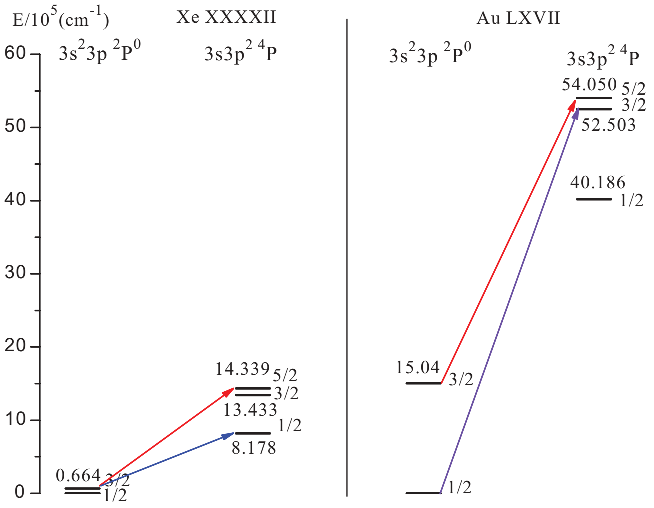

FIG. 2. (Color online) Calculated levels for the lowest five levels of Al-like ions of Xe ($Z = 54$, left) and Au ($Z = 79$, right).

as in many isoelectronic sequences, but only with data for $Z \leqslant 42$. By combining this extensive MCDHF of calculations with the results of experimental material of Jupén *et al.* [1], it would be interesting to follow these changes in detail in order to verify one or the other interpretation and to study the details of the available relativistic calculations as a function of Z; reliable interpolations and extrapolations are possible. Thus, the small differences between the theoretical and experimental energies, which vary slowly and smoothly with Z, were fitted to a fourth-degree polynomial in Z. However, with the experimental results now available up to Mo XXX, reasonably reliable extrapolations up to Xe XXXXII are possible. Such extrapolations are best achieved by studying the Z dependence of the difference between experimental and theoretical transition energies. Further experimental confirmation would be very helpful in verifying the correctness of these occasionally sensitive mixing parameters.

Five lines of the doublet system were found for most of the ions studied. These determine the levels of the $3s^23p$ and $3s3p^2$ configurations. Tables V–IX each contain the lines of one isoelectronic transition, including the measured and calculated energy values. Comparisons of our MCDHF energies with other theoretical and experimental data are too voluminous to include here but are available as experimental data are taken as reported by Jupén *et al.* [3], Sugar *et al.* [7], Ekberg *et al.* [4], and researchers at NIST. Predicted data based on measurements has been given by Froese Fischer *et al.* [9], Safronova *et al.* [16], and Vilkas *et al.* [17,18]. Similar data for Fe XIV and Ni XVI were given by Gupta *et al.* [13] and Aggarwal *et al.* [37]. As can be seen in Tables V–IX, our results are in excellent agreement with the predicted data, the difference being 0.01%–1% for most cases. It should be noted that relativistic MCDHF calculation are more accurate for high-Z ions. Good agreement with experimental data obtained for low-Z ions leads us to conclude that the MCDHF method can provide accurate energies for all values of Z. Our MCDHF results are in excellent agreement with NIST data for Fe through Mo, the difference being about 0.008%–0.1% for most cases. The deviations between the present values and the experimental determinations suggest that additional correlation effects must be taken into account to reduce the discrepancy.

In Table X, we give A values, lifetimes, and branching ratios for the MCDHF methods, discussed previously. We compare these results with those from other experiments. It is interesting to note that experimental results for Q agree with ours to within a couple of percent. The lifetime appears to be a slowly converging property within a given model, while the Q value, in comparison, converges very quickly and can be estimated to a good accuracy from relatively small calculations. Together these two properties constitute an excellent test for atomic structure calculations.

In order to check the reliability of our calculation, we compare our results for wavelengths λ, transition probabilities A, and line strengths S in length L and velocity V forms for

TABLE V. Fine-structure energy levels (in cm^{-1}) for the $3s^23p\ ^2P_{3/2}$ level for different ions in the aluminum like isoelectronic sequence, from present calculations and compared with experiments and theoretical results.

Z	VV	CV	CC	NIST[a]	Expt.[b]	MBPT[c]	CIV3[d]	MCHF[e]
26	18773	18835	18845	18852.5	18852	18684	18793.9	18766.34
28	27665	27744	27739	27760.4	27756	27731	27752.4	27626.3[f]
34	73485	73631	73556	73640	73626	73555		
36	97176	97337	97241	97312	97322	97281		
40	161511	161734	161554	161680[g]	161680			
42	203845	204106	203877	204020	204048	203906		
54	665848	666349	665955			665774[h]		
79	1505306	1505039	1504660			1504645[i]		

[a] Taken from [34].
[b] Jupén and Curtis [3].
[c] Safronova *et al.* [16].
[d] Gupta *et al.* [13].
[e] Froese Fischer *et al.* [9].
[f] Aggarwal *et al.* [37].
[g] Ekberg and Redfors [4].
[h] Vilkas *et al.* [17].
[i] Vilkas *et al.* [18].

TABLE VI. Fine-structure energy levels (in cm^{-1}) for the $3s3p^2\,{}^4P_{1/2}$ level for different ions in the aluminum like isoelectronic sequence, from present calculations and compared with experiments and theoretical results.

Z	VV	CV	CC	NIST[a]	Expt.[b]	MBPT[c]	CIV3[e]	MCHF[e]
26	223923	224452	223385	225114	225083	225187	225125.9	223427.79
28	258325	258881	257852	259489	259472	259627	259467.2	257190.4[f]
34	370683	371438	370434	371506[g]	371658	37244		
36	411100	411668	410944	411750	411903	411898		
40	495702	496213	495758	495631[g]	495754			
42	539590	539349	539744	538435	538930			
54	818362	818437	819114			817897[h]		
79	4017333	4018744	4021257			4013023[i]		

[a] Taken from [34].
[b] Jupen and Curtis [3].
[c] Safronova *et al.* [16].
[e] Gupta *et al.* [13].
[e] Froese Fischer [9].
[f] Aggarwal *et al.* [37].
[g] Ekberg and Redfors [4].
[h] Vilkas *et al.* [17].
[i] Vilkas *et al.* [18].

Al-like ions with nuclear charges ranging from $Z = 26$ to 79 (Table XI). Also some available theoretical and experimental results are tabulated for comparison. Our comparison is presented in two parts: wavelengths and transition probability differences. Our MCDHF values are compared with theoretical values given by Froese Fischer *et al.* [9], by Safronova *et al.* [43], and by Vilkas *et al.* [17,18] and experimental results given by Jupén *et al.* [1], by Sugar and Kaufman [7], by Jupén and Curtis [3], and by researchers at NIST [34]. For medium- to low-Z ions (Table XI), it is clear that the calculated values including the CV correlation are in general in very good agreement with the MCHF calculations of Froese Fischer *et al.* [9] and the MBPT calculations of Safronova *et al.* [43] and Vilkas *et al.* [17,18] except for some transitions with a maximum difference of approximately 0.4%, but the maximum difference for our VV correlation calculations is 0.8%. A comparison between the present wavelengths and the JET tokamak experimental values of Jupén *et al.* [1], Sugar and Kaufman [7], and Jupén and Curtis [3] and the observations of NIST [34] reveals that the greatest difference between the experimental results and our GRASP2K transition wavelengths for our CV correlation calculations is 0.25% and the maximum difference for the results of VV correlation calculations is 0.5%. However, a more detailed comparison of the calculated and observed wavelengths for these transitions for high-Z ions (Table XI) indicates that the transition wavelengths given by

TABLE VII. Fine-structure energy levels (in cm^{-1}) for the $3s3p^2\,{}^4P_{3/2}$ level for different ions in the aluminum like isoelectronic sequence, from present calculations and compared with experiments and theoretical results.

Z	VV	CV	CC	NIST[a]	Expt.[b]	MBPT[c]	CIV3[d]	MCHF[e]
26	231555	232112	231009	232789	232470	232889	232894.3	231238.10
28	270120	270718	269619	271341	271247	271526	271433.6	268918.7[f]
34	407670	408576	407277	408749[g]	409934			
36	462914	463662	462547	464204	465300	464088		
40	591950	592786	591638	592888[g]	592888			
42	667489	668428	667182	668752[h]	666293			
54	1342192	1343346	1342108			1343238[i]		
79	5249361	5251590	5247237			5247290[j]		

[a] Taken from [34].
[b] Jupén and Curtis [3].
[c] Safronova *et al.* [16].
[d] Gupta *et al.* [13].
[e] Froese Fischer [9].
[f] Aggarwal *et al.* [37].
[g] Ekberg and Redfors [4].
[h] Jupén *et al.* [1].
[i] Vilkas *et al.* [17].
[j] Vilkas *et al.* [18].

TABLE VIII. Fine-structure energy levels (in cm^{-1}) for the $3s3p^2\,{}^4P_{5/2}$ level for different ions in the aluminum like isoelectronic sequence, from present calculations and compared with experiments and theoretical results.

Z	VV	CV	CC	NIST[a]	Expt.[b]	MBPT[c]	CIV3[d]	MCHF[e]
26	241155	241733	240669	242387	242332	242451	242432.7	240683.01
28	283743	284360	283326	284949	284858	285072	284920.0	282563.1[f]
34	437883	438768	437735	438805[g]	438821			
36	499611	500343	499574	500480(75)[h]	500593	500343		
40	641776	642559	641977	642359[g]	642715			
42	723690	724546	723987	724522[h]	724101			
54	1433350	1434253	1434213			1433127[i]		
79	5412380	5413777	5433071			5408298[j]		

[a] Taken from [34].
[b] Jupén and Curtis [3].
[c] Safronova *et al.* [16].
[d] Gupta *et al.* [13].
[e] Froese Fischer *et al.* [9].
[f] Aggarwal *et al.* [37].
[g] Ekberg and Redfors [4].
[h] Jupén *et al.* [1].
[i] Vilkas [17].
[j] Vilkas *et al.* [18].

our VV calculations are in better agreement with the accurate calculations of Vilkas *et al.* [17,18] than our CV correlation results. The maximum difference between the accurate results of Vilkas *et al.* [17,18] and our VV transition wavelengths is 0.03%, but the maximum difference for our CV results and those calculated by Vilkas *et al.* [17,18] is 0.04%. For this transition the wavelengths obtained by the two models are very close. It is most likely that this is due to slower convergence of the correlation treatment for GRASP2K, since the effect decreases for higher Z. The calculations are fundamentally different and a comparison between the different models employed merely indicates the main similarities, and only the final converged values can be critically compared. To avoid future level identification problems, besides wavelengths we include in Table XI transition rates A and line strength S.

In view of the VV and CV correlation independence just discussed, our transition rate results are presented in CV correlation form only. Uncertainties in the accuracy of the A values for these transitions will be determined mainly by the accuracy of the line strength S. Our GRASP2K calculation of the A value for the $3s^2 3p$-$3s3p^2$ transition is in excellent agreement with the theoretical and experimental results. In Table XI, we illustrate the Z dependence of the differences between line strengths calculated in length S_L and velocity S_V forms. The agreement between the theoretical L form and the$V$ form results were also used in [9,43] as an indicator of accuracy. Since the present transition data are obtained using a single method for all Z, and improve in accuracy with increasing Z, we expect our data for high Z to be very reliable.

TABLE IX. Fine-structure energy levels (in cm^{-1}) for the $3s3p^2\,{}^2D_{3/2}$ level for different ions in the aluminum like isoelectronic sequence, from present calculations and compared with experiments and theoretical results.

Z	VV	CV	CC	NIST[a]	Expt.[b]	MBPT[c]	CIV3[d]	MCHF[e]
26	299689	300636	301031	299242	299247[f]	298903	298407.9	299078.23
28	347574	348517	348914	347032		346780	346099.2	347783.8[g]
34	514934	515878	516251	514130[h]	514128			
36	580722	581641	582018	579737(120)[i]	579808	579451		
40	731515	732401	732806	730348[h]	730340			
42	818134	819074	819456	816880(100)[i]	816860			
54	2332472	2336124	2341023			2332373[j]		
79	5590890	5593645	5607532			5586504[k]		

[a] Taken from [34].
[b] Sugar and Kaufman [7].
[c] Safronova *et al.* [16].
[d] Gupta *et al.* [13].
[e] Froese Fischer *et al.* [9].
[f] Redfors and Litzén [5].
[g] Aggarwal *et al.* [37].
[h] Ekberg and Redfors [4].
[i] Jupén *et al.* [1].
[j] Vilkas *et al.* [17].
[k] Vilkas *et al.* [18].

TABLE X. Properties for the $3s^2 3p\ ^2P_J$–$3s3p^2\ ^2S_{1/2}$ transition, for different ions in the aluminum like isoelectronic sequence, from present calculations and compared with experiment.

Z	$A_1(^2P_{1/2}\text{-}^2S_{1/2})$ (10^8 s^{-1})	$A_2(^2P_{3/2}\text{-}^2S_{1/2})$ (10^8 s^{-1})	Q_A[a]	Q (Expt.)	Theory[c] (ps)	Expt.[d] (ps)
26	182.70	10.10	0.055	0.060 ± 0.01[b]	51.867	52.083
28	263.64	3.66	0.014	0.0146[d]	37.411	37.908
34	540.46	6.55	0.012		18.281	
36	651.95	13.60	0.021		15.025	
40	920.97	32.18	0.035		10.492	
42	1094.65	43.71	0.040		8.785	
54	3233.22	128.31	0.040		2.975	
79	48530.08	377.15	0.008		0.204	

[a] Branching ratios of transition rates, $Q_A = A(3s^2 3p\ ^2P_{3/2}\text{–}3s3p^2\ ^2S_{1/2})/A(3s^2 3p\ ^2P_{1/2}\text{–}3s3p^2\ ^2S_{1/2})$.

[b] Taken from [42].

[c] Present results from the core–valence correlation, $n = 7$ calculations.

[d] The experimental results are those we calculated from Ref. [34].

TABLE XI. Wavelengths (in angstroms), line strengths, and transition probabilities in different Al-like ions in different approaches, compared to experiments and theories. Numbers in square brackets denote powers of 10.

	Previous	Present λ (Å)			S_L	S_V CV	Previous	Present A (s^{-1})		
Z	λ (Å)	VV	CV	CC	CV	CV	A(s^{-1})	VV	CV	CC
					$3s^2 3p\ ^2P_{1/2}$–$3s3p^2\ ^4P_{1/2}$					
26	447.57[a]	446.58	446.48	447.81	2.10[−3]	2.20[−3]	2.62(7)[a]	2.54(7)	2.59(7)	2.29(7)
28	385.37[b]	386.23	386.14	386.82	3.05[−3]	3.18[−3]	5.7(7)[b]	5.39(7)	5.57(7)	5.16(7)
34	268.91[c]	268.78	268.90	268.95	7.75[−3]	7.50[−3]		3.88(8)	3.86(8)	3.77(8)
36	242.56[c]	243.26	243.16	243.34	9.43[−3]	9.75[−3]		6.83(8)	6.73(8)	6.52(8)
40		201.74	201.74	201.71	1.37[−2]	1.35[−2]		1.71(9)	1.69(9)	1.65(9)
42	185.53[f]	185.43	185.41	185.28	1.54[−2]	1.59[−2]		2.47(9)	2.45(9)	2.43(9)
54	122.27[g]	122.26	122.28	122.08	2.06[−2]	2.08[−2]	1.15(10)[g]	1.15(10)	1.16(10)	1.15(10)
79	66.46[h]	66.43	66.49	66.46	1.33[−2]	1.43[−2]	4.65(10)[h]	4.68(10)	4.60(10)	4.83(10)
					$3s^2\ 3p^2\ P_{1/2}$–$3s3p^2\ ^2P_{1/2}$					
26	255.42[a]	254.54	255.78	253.88	2.54[−1]	2.48[−1]	1.51(10)[a]	1.53(10)	1.27(10)	1.40(10)
28	223.13[b]	221.36	222.83	221.30	1.21[−1]	1.15[−1]	1.3(10)[b]	1.38(10)	1.12(10)	1.22(10)
34	150.32[e]	149.40	149.62	148.96	2.36[−2]	2.24[−2]	7.84(9)[e]	8.56(9)	7.16(9)	7.72(9)
36	132.56[e]	131.80	131.96	131.44	1.70[−2]	1.68[−2]	6.90(9)[e]	7.43(9)	6.35(9)	6.79(9)
40	124.02[d]	123.62	123.94	123.40	1.72[−1]	1.71[−1]		9.35(10)	9.1110)	9.24(10)
42	112.17[d]	111.58	111.89	111.47	1.51[−1]	1.53[−1]		1.32(11)	1.09(11)	1.12(11)
54	61.62[g]	61.56	61.55	61.39	7.43[−2]	7.46[−2]	3.30(11)[g]	3.28(11)	3.23(11)	3.28(11)
79		17.58	17.59	17.55	2.63[−2]	2.65[−2]		4.94(12)	4.85(12)	4.99(12)
					$3s^2\ 3p^2\ P_{1/2}$–$3s3\ p^2\ ^2P_{3/2}$					
26	250.01[a]	249.15	250.78	248.79	2.29[−1]	2.21[−1]	7.90(9)[a]	8.01(9)	7.36(9)	7.76(9)
28	218.38[b]	217.97	218.27	217.64	1.86[−1]	1.80[−1]	9.5(9)[b]	1.00(10)	9.18(9)	9.73(9)
34	147.75[e]	146.52	147.12	146.38	1.16[−1]	1.13[−1]	2.08(10)[e]	2.14(10)	1.90(10)	2.05(10)
36	130.78[e]	129.74	130.18	129.62	1.13[−1]	1.10[−1]	2.92(10)[e]	2.99(10)	2.61(10)	2.84(10)
40	103.35[e]	102.69	102.92	102.54	1.37[−1]	1.35[−1]	7.13(10)[e]	7.23(10)	6.38(10)	6.77(10)
42	92.59[e]	92.04	91.90	91.85	1.67[−1]	1.68[−1]	1.13(11)[e]	1.15(11)	1.01(11)	1.09(11)
54	64.20[g]	64.12	64.11	64.06	4.68[−2]	4.82[−2]	8.39(10)[g]	8.88(10)	8.99(10)	8.79(10)
79	16.49[e]	16.45	16.43	16.35	5.64[−2]	5.66[−2]	6.69(12)[e]	6.60(12)	6.43(12)	6.93(12)
					$3s^2\ 3p^2\ P_{3/2}$–$3s3p^2\ ^4P_{3/2}$					
26	470.65[a]	470.00	470.40	471.40	1.22[−3]	1.22[−3]	5.91(6)[a]	5.94(6)	5.90(6)	5.62(6)
28	410.54[b]	410.47	410.32	411.13	1.61[−3]	1.61[−3]	1.15(7)[c]	1.16(7)	1.17(7)	1.12(7)
34	298.20[c]	298.25	298.18	298.65	2.94[−3]	2.98[−3]		5.29(7)	5.16(7)	5.02(7)
36	272.54[c]	272.43	272.48	272.74	3.37[−3]	3.42[−3]		8.29(7)	8.31(7)	8.05(7)
40		232.33	232.31	232.51	4.11[−3]	4.26[−3]		1.65(8)	1.66(8)	1.61(8)
42		215.70	215.84	215.85	4.36[−3]	4.40[−3]		2.19(8)	2.18(8)	2.15(8)

TABLE XI. *(Continued.)*

	Previous	Present λ (Å)			S_L	S_V CV	Previous	Present A (s^{-1})		
Z	λ (Å)	VV	CV	CC	CV	CV	A(s^{-1})	VV	CV	CC
54	147.61[g]	147.86	147.87	147.90	4.61[−3]	4.90[−3]	7.18(8)[g]	7.23(8)	7.23(8)	7.15(8)
79	81.02[h]	81.16	81.18	81.56	2.57[−3]	2.90[−3]	2.38(9)[h]	2.43(9)	2.43(9)	3.24(9)
					$3s^2\,3p^2\ P_{1/2}$–$3s3\ p^2\ {}^2D_{3/2}$					
26	334.36[a]	333.67	334.19	333.52	1.84[−1]	1.90[−1]	2.46(9)[a]	2.45(9)	2.55(9)	2.42(9)
28	288.15[b]	287.70	287.48	287.60	1.60[−1]	1.64[−1]	3.2(9)[b]	3.32(9)	3.44(9)	3.28(9)
34	194.51[e]	194.20	194.48	193.70	1.13[−1]	1.15[−1]	6.92(9)[e]	7.70(9)	7.01(9)	7.58(9)
36	172.58[e]	172.20	172.70	171.82	1.03[−1]	1.04[−1]	9.05(9)[e]	1.00(10)	9.23(10)	9.88(9)
40	136.98[e]	136.70	136.82	136.46	8.58[−2]	8.81[−2]	1.53(10)[e]	1.67(10)	1.58(10)	1.65(10)
42	122.47[e]	122.23	122.35	122.03	7.87[−2]	7.96[−2]	1.97(10)[e]	2.15(10)	2.09(10)	2.12(10)
54	64.20[g]	64.12	64.08	64.11	4.69[−2]	4.79[−2]	8.08(10)[e]	8.86(10)	9.03(10)	8.99(10)
79	17.91[e]	17.89	17.88	17.52	1.45[−2]	1.50[−2]	1.02(12)[e]	1.24(12)	1.28(12)	1.14(12)
					$3s^2\,3p^2\ P_{3/2}$–$3s3p^2\ {}^4P_{5/2}$					
26	450.62[a]	449.71	449.99	450.91	6.56[−3]	6.82[−3]	2.49(7)[a]	2.56(7)	2.43(7)	2.33(7)
28	388.82[b]	389.53	389.74	390.26	9.63[−3]	9.85[−3]	5.6(7)[b]	5.71(7)	5.45(7)	5.27(7)
34	273.79[c]	273.44	273.50	273.59	2.29[−2]	2.38[−2]		3.86(8)	3.75(8)	3.65(8)
36	248.07[c]	248.10	248.12	248.15	2.76[−2]	2.86[−2]		6.14(8)	6.08(8)	5.94(8)
40		208.22	208.21	208.15	3.50[−2]	3.75[−2]		1.31(9)	1.31(9)	1.26(9)
42	192.26[e]	192.38	192.35	192.27	3.62[−2]	3.77[−2]		1.75(9)	1.72(9)	1.69(9)
54	130.32[g]	130.29	130.34	130.16	3.30[−2]	3.62[−2]	4.95(9)[g]	5.07(9)	5.03(9)	4.99(9)
79	71.67[h]	71.68	71.74	70.83	1.87[−2]	2.17[−2]	1.70(10)[h]	1.73(10)	1.71(10)	2.55(10)

[a] Calculation of Froese Fischer *et al.* [9].
[b] Taken from [34].
[c] Experimental results of Jupén *et al.* [1].
[d] Experimental results of Sugar and Kaufman [7].
[e] Calculation of Safronova*et al.* [43].
[f] Experimental results of Jupén and Curtis [3].
[g] Calculation of Vilkas *et al.* [17].
[h] Calculation of Vilkas *et al.* [18].

VI. SUMMARY

We report on relativistic multiconfiguration Dirac-Hartree-Fock calculations of fine-structure energy levels, the term splitting, the wavelengths, transition rates, line strengths, and thereby the branching ratios and lifetimes of the aluminum like $3s^23p$-$3s3p^2$ transitions in the ions Fe XIV–Au LXVII. We show different results for fine-structure energies from methods including different effects. The MCDHF gives excellent agreement with experimental data and adopted results. It would be beneficial if experimental data for other highly charged Al-like ions were available. At the present time, there are no experimental data between $Z \geqslant 43$ and $Z \leqslant 100$ for the aluminum isoelectronic sequence. Availability of such data would lead to an improved understanding of the relative importance of different contributions to the energies of highly charged ions. In addition, we estimate that the uncertainties are about 10% for the GRASP2K calculations. The influence of the core-valence correlation on the lifetime and branching ratio were discussed. These calculations provide a theoretical benchmark for comparison with experiment and theory. It is found that the relativistic and configuration interaction effects play an important role in the correct assignment of different transitions and also in the accurate evaluation of atomic transition data of highly ionized atoms. For low-Z (see Tables IV–IX) ions it is clear that the MCDHF method, including the core-valence correlation, is an accurate approach for the whole sequence and that calculations including only the valence correlation and the core-core correlation underestimate the energy levels. The agreement with NIST data, including only the core-core correlation, shows that this might be fortuitous. Since the discrepancy is not clear as atomic number Z increases, further experimental investigation is of great interest to explain the difference between theoretical and experimental results, especially for large Z values. It is in general clear that these kinds of transitions require much work, especially on the experimental side, to explain the differences among different computational methods and to facilitate their use in plasma diagnostics. However, because these results are all from single- or few-configuration calculations, it would be imprudent to conclude that it is presently more than a trend; more calculations with more configurations are clearly in order. We hope that these results will be useful in analyzing older experiments and planning new ones.

ACKNOWLEDGMENTS

The authors are grateful to P. Jönsson for providing the GRASP2K package and ATSP2K package and giving us many useful instructions. This work was supported by the Nation 863 High-tech Project Fund.

[1] C. Jupén, B. Denne, and I. Martinson, Phys. Scr. **41**, 669 (1990).
[2] U. Litzén and A. Redfors, Phys. Lett. **A127**, 88 (1988)
[3] C. Jupén and L. J. Curtis, Phys. Scr. **53**, 312 (1996).
[4] J. O. Ekberg and A. Redfors, Phys. Scr. **44**, 539 (1991).
[5] A. Redfors, U. Litzén, J. Opt. Soc. Am. B **6**, 1447 (1989).
[6] C. Corliss and J. Sugar, J. Phys. Chem. Ref. Data **11**, 135 (1982).
[7] J. Sugar and V. Kaufman, J. Opt. Soc. Am. B **5**, 10 (1988).
[8] S. S. Tayal, J. Phys. B **40**, 2551 (2007).
[9] C. Froese Fischer, G. Tachiev, and A. Irimia, At. Data Nucl. Data Tables **92**, 607 (2006).
[10] G. P. Gupta and A. Z. Msezane, Eur. Phys. J. D **49**, 157 (2008).
[11] G. P. Gupta and A. Z. Msezane, Phys. Scr. **76**, 225 (2007).
[12] K. B. Choudhury, N. C. Deb, K. Roy, and A. Z. Msezane, Eur. Phys. J. D **27**, 103 (2003).
[13] G. P. Gupta and A. Z. Msezane, At. Data Nucl. Data Tables **89**, 1 (2005).
[14] G. P. Gupta and A. Z. Msezane, Astrophys. J. Suppl. Ser. **130**, 227 (2000).
[15] G. P. Gupta and A. Z. Msezane, Phys. Scr. **69**, 273 (2004).
[16] U. I. Safronova, C. Namba, J. R. Albritton, W. R. Johnson, and M. S. Safronova, Phys. Rev. A **65**, 022507 (2002).
[17] M. J. Vilkas, Y. Ishikawa, and E. Träbert, J. Phys. B **39**, 2195 (2006).
[18] M. J. Vilkas, Y. Ishikawa, and E. Träbert, Eur. Phys. J. D **41**, 77 (2007).
[19] E. Landi, P. J. Storey, and C. J. Zeippen, Astrophys. J. **607**, 640 (2004).
[20] E. Biémont *et al.*, Eur. Phys. J. D **40**, 91 (2006).
[21] E. Charro and I. Martín, Astrophys. J. Suppl. Ser. **126**, 551 (2000).
[22] F. Hu, G. Jiang, W. Hong, and L.-H. Hao, Eur. Phys. J. D **49**, 293 (2008).
[23] L.-H. Hao, G. Jiang, S.-Q. Song, and F. Hu, At. Data Nucl. Data Tables **94**, 739 (2008).
[24] I. P. Grant, *Relativistic Quantum Theory of Atoms and Molecules* (Springer, New York, 2007).
[25] I. P Grant, B. J McKenzie, P. H. Norrington, D. F. Mayers, and N. C. Pyper, Comput. Phys. Commun. **21**, 207 (1980).
[26] P. Jönsson, X. He, C. Froese Fischer, and I. P. Grant, Comput. Phys. Commun. **177**, 597 (2007).
[27] F. A. Parpia, C. Froese Fischer, and I. P. Grant, Comput. Phys. Commun. **94**, 249 (1996).
[28] J. Olsen, M. R. Godefroid, P. A. Jonsson, P. A. Malmquist, and F. C. Froese, Phys. Rev. E **52**, 4499 (1995).
[29] C. Froese Fischer, T. Brage, and P. Jönsson, *Computational Atomic Structure* (Institute of Physics, Bristol, 1997).
[30] B. J. McKenzie, I. P. Grant, and P. H. Norrington, Comput. Phys. Commun. **21**, 233 (1980).
[31] S. Q. Song, F. Peng, and G. Jiang, J. Phys. B **39**, 2087 (2006).
[32] P. H. Norrington, A. E. Kingston, and A. W. Boone, J. Phys. B **33**, 1767 (2000).
[33] A. K. Bhatia and G. A. Doschek, At. Data Nucl. Data Tables **71**, 69 (1999).
[34] The NIST atomic spectra collection, http://physics.nist.gov/PhysRefData/ASD/levels_form.html.
[35] D. McPeake and A. Hibbert, J. Phys. B **33**, 2809 (2000).
[36] P. Jönsson, C. Froese Fischer, and M. R. Godefroid, J. Phys. B **32**, 1233 (1999).
[37] K. M. Aggarwal, F. P. Keenan, and A. Z. Msezane, At. Data Nucl. Data Tables **85**, 453 (2003).
[38] E. Trabert., P. H. Heckmann, R. Hutton., and I. Martinson, J. Opt. Soc. Am. B **5**, 2173 (1988).
[39] D. G. Ellis, I. Martinson, and E. Trabert, Comments At. Mol. Phys. **22**, 241 (1989).
[40] K. N. Huang, At. Data Nucl. Data Tables **34**, 1 (1986).
[41] A. Farrag, E. Luc-Koenig, and J. Sinzelle, At. Data Nucl. Data Tables **27**, 539 (1982).
[42] L. Engström *et al.*, Phys. Scr. **52**, 516 (1995).
[43] U. I. Safronova, M. Sataka, J. R. Albritton, W. R. Johnson, and M. S. Safronova, At. Data Nucl. Data Tables **84**, 1 (2003)